Photon energy and polarization-dependent electronic structure of Cr-doped Bi_{2}Se_{3}

T. Yilmaz, G. D. Gu, E. Vescovo, K. Kaznatcheev, and B. Sinkovic

Phys. Rev. Materials **4**, 024201 — Published 5 February 2020

DOI: 10.1103/PhysRevMaterials.4.024201

Photon energy and polarization dependent electronic structure of Cr doped Bi_2Se_3

T. Yilmaz,[1] G. D. Gu,[2] E. Vescovo,[1] K. Kaznatcheev,[1] and B. Sinkovic[3]

[1]*National Synchrotron Light Source II, Brookhaven National Lab, Upton, New York 11973, USA*
[2]*Condensed Matter Physics and Materials Science Department, Brookhaven National Lab, Upton, New York 11973, USA*
[3]*Department of Physics, University of Connecticut, Storrs, Connecticut 06269, USA*

(Dated: January 15, 2020)

In this article, we reported a comparative study of the electronic structure of Cr doped and pristine Bi_2Se_3. Circular dichroism and photon energy dependent angle resolved photoemission experiments were performed. Even though the surface states seen on the Cr doped samples are gapped, they exhibit strong circular dichroism, for which we provide its origin in accordance with the non-trivial band structure of the bulk. The surface electronic structure measurements with linear and circular polarized light show signature that the orbital composition of the surface states is changed with Cr doping. Our observations not only provide further spectroscopic information about topological materials but also promotes an alternative experimental tool to control their spin-orbital texture.

Topological insulators (TIs) are the new quantum states of the matter that exhibit cone like electronic structure with a gapless Dirac point (DP) formed by the linear topological surface states (TSSs). Unlike the conventional insulators, the bulk band gap in a TI is inverted due to the strong spin orbit coupling (SOC) [1-5]. Also, the spin and the momentum of the surface electrons in a TI are locked perpendicular to each other. This peculiar electronic structure manifests helical spin texture and differs from normal insulators with a Z2 invariant number. Furthermore, these surface states are protected against the non-magnetic perturbations by time-reversal symmetry (TRS) ($E(\boldsymbol{k},\uparrow) = E(\text{-}\boldsymbol{k},\downarrow)$) which forbids the backscattering of the Dirac electrons and guarantees the helical spin texture [5-9]. After the theoretical predictions, angle-resolved photoemission spectroscopy (ARPES) studies confirmed the existence of the TSSs in Bi_2Se_3 and Bi_2Te_3 with a single Dirac cone at the $\overline{\Gamma}$ point of the Brillouin zone (BZ) [10-12].

One of the particular interest in TIs is to investigate the correlation between magnetic impurities and the TSSs. In the presence of a net out-of-plane magnetic moment, TRS can be broken and the dissipationless one dimensional chiral edge states can be formed at the sample boundaries which leads to the emergence of the quantum anomalous Hall effect (QAHE) [13-14]. In recent works, the QAHE was observed in V and Cr doped (Bi,Sb)Te TI [15-16], but limited to few Kelvin due to the details of the electronic structure, such as bulk band crossing the Fermi level (E_F) [17]. There is also a tremendous interest on the band structure of the magnetic impurity doped TIs since the QAHE manifests itself as an energy gap opening at the DP. Therefore, along with the transport measurements, numerous ARPES studies have been reported on Cr, Mn, V, and Fe doped Bi_2Se_3 and Bi_2Te_3 to observe the magnetic gap at the DP [18-27]. Although its origin of the gap is still under debate; for example, some groups attribute the gap to the ferromagnetic orders [18-19], while others claimed it to be originated from the impurity resonant states [30-32]. The manipulation of the spin-orbital texture of the TSSs is the key factor for the spin-based devices. Therefore, further experimental studies are essential to understand the interplay of the TSSs and the magnetic impurities to enable the high temperature QAHE.

Hence, in the present work, we measure the surface electronic structure of Cr doped Bi_2Se_3 ($Bi_{1.78}Cr_{0.22}Se_3$) by performing photon energy and photon polarization dependent ARPES experiments. Then, compare its electronic structure with the pristine Bi_2Se_3 for the same experimental geometry. Our photon energy dependent ARPES experiment along with the circular dichroism in ARPES implies the persistence of the TSSs in Bi_2Se_3 against Cr doping. Furthermore, comparative ARPES data taken from Cr doped and pristine samples collected with s- and p-polarized lights provides signature for the modified orbital composition of the TSSs in Bi_2Se_3 with Cr doping. The present work applies the variable experimental geometry in photoemission of transition metal doped TIs. Therefore, our findings should play an important role for understanding and manipulation of the TSSs.

To obtain well ordered Cr doped thin film samples to study in ARPES, we grow 3 quintuple layers (QLs) $Bi_{1.78}Cr_{0.22}Se_3$ on a 12 QL pristine Bi_2Se_3 by using molecular beam epitaxial method (MBE). We realized that the heterostructure as schematically presented in Figure 1(a) suppresses the disorder induced broadening of the bands in ARPES even though the sample is highly Cr doped. The MBE grown samples were capped with 15 nm Se to protect them in atmosphere. The films were transferred into the ARPES chamber and annealed at 250 C^o for an hour to remove the Se-capping layer. This annealing procedure was tested with high resolution core level spectroscopy to confirm the absence of the Se metal on the sample surface or the formation of the chemically different environments than Cr doped Bi_2Se_3. For the pristine sample, we used single crystal Bi_2Se_3 grown by floating zone method. The single crystals were cleaved in the ARPES chamber before the photoemission experiment. Photon energy and polarization dependent ARPES experiments were performed at 21ID-I ESM

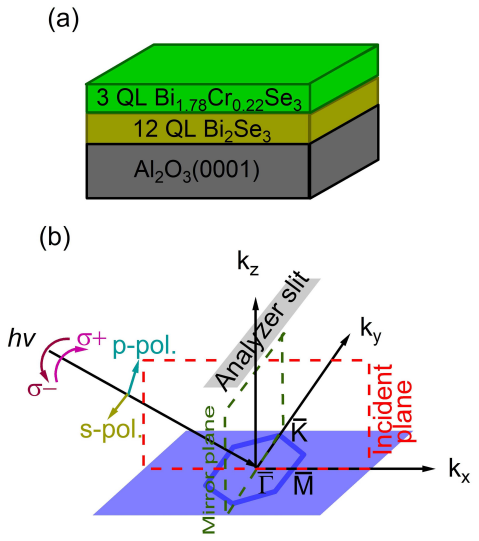

FIG. 1. (a) Sycematic representattion of the studied sample. (b) Experimental geometry for photoemission experiment.

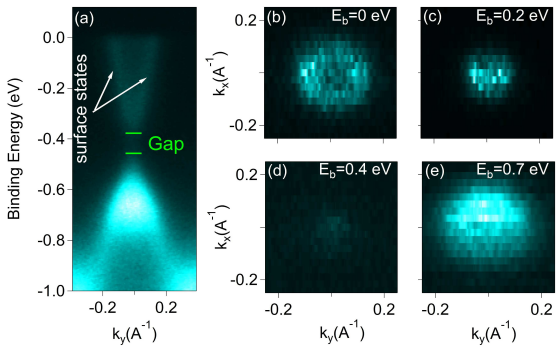

FIG. 2. (a) ARPES map of the $Bi_{1.78}Cr_{0.22}Se_3$ thin film taken with 50 eV p-pol. light at 15 K. (b-e) Constant energy counters at different E_b.

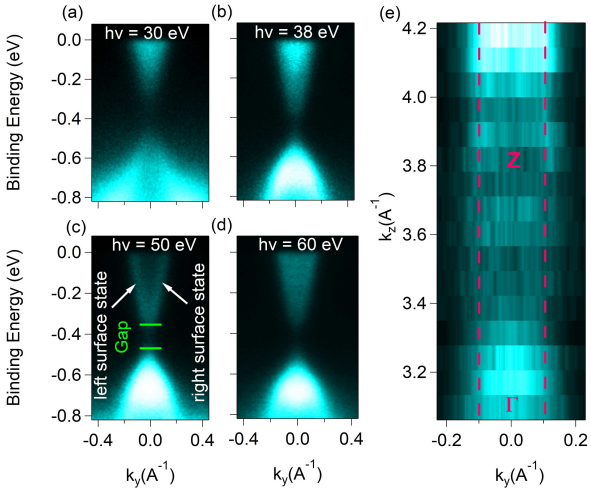

FIG. 3. (a - d) Photon energy dependent surface electronic structure of $Bi_{1.78}Cr_{0.22}Se_3$. (e) ARPES intensity plot in the k_z-k_y plane at E_F.

beamline of National Synchrotron Light Source II (NSLS-II) by using DA30 Scienta electron spectrometer. The angle between the light and the surface normal is 55^o at the normal emission as indicated in Figure 1(b). The pressure in the photoemission chamber was $1x10^{-11}$ torr and samples were kept at 15 K during the experiment by a closed cycle He cryostat.

The surface electronic structure of the $Bi_{1.78}Cr_{0.22}Se_3$ thin film sample is given in Figure 2(a). The spectrum is collected with p-polarized 50 eV photons along the $\overline{\Gamma}$ - $\overline{K}$ direction of the BZ. The band structure exhibits an energy gap of 0.1 eV between the bottom and the upper surface states of the Dirac cone as indicated with green lines in Figure 2(a). Since the spectrum is obtained above the ferromagnetic transition temperature of 10 K [28], the gap should not be due to the ferromagnetic order. The non-magnetic gap in the surface electronic structure of a TI has been proposed to be induced by the impurity states that strongly modify the Dirac cone [29-32]. Figure 2(b-e) gives the constant energy counters at various binding energies. A notable spectral feature of the energy cuts is that the non-uniform photoemission intensity is observed around the measured energy counters. A similar observation was also reported for the pristine Bi_2Se_3 in which the surface states are dominated by the p_z orbitals [33]. This demonstrates that the surface states in Cr doped Bi_2Se_3 is also formed by mainly the p_z orbitals.

To study the band dispersion along the k_z direction of the BZ in $Bi_{1.78}Cr_{0.22}Se_3$, we conducted ARPES maps with photon energies ranging from 30 eV to 60 eV (Figure 3). By using $\hbar k_z=[2m_e(E_{kin}\cos^2\theta - V_0)]^{1/2}$ where m_e is the electron mass, E_{kin} is the kinetic energy of a photoelectron, and the inner potential $V_0 = 11.7$ eV [12], 30 eV and 50 eV photon energies match with the vicinity of the Γ and Z-point of the BZ, respectively. At the Γ point, the bulk conduction band has the lowest binding energy (E_b) [4] leading a strong overlapping between the surface states and the bulk bands (Figure 3(a)). With increasing photon energy in Figure 3(b-d), the bulk conduction band exhibits strong k_z dependence while surface states are present at all photon energies due to its two dimensional nature. This can be better seen in k_z versus k_y ARPES plot at the E_F in Figure 3(e) where the non-dispersive surface states are marked with straight dashed lines. Also, the bulk bands are resolved around $k_z = 3.1$ Å^{-1} and 4.2 Å^{-1}. Hence, our photon energy dependent ARPES confirms the persistence of the 2D surface states in Bi_2Se_3 against high Cr doping level.

After revealing the surface states, we turned our attention to resolve the orbital texture of surface states in highly Cr doped Bi_2Se_3. This could be achieved by taking advantage of the polarized photons. The spectral weight in photoemission experiment strongly depends on the "transition matrix elements" given by $< f\ |\mathbf{E}\cdot\mathbf{r}|\ i >$

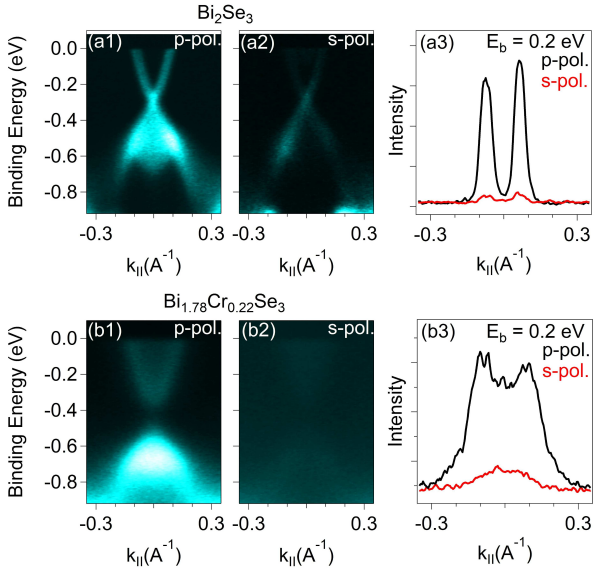

FIG. 4. (a1-a2) Surface electronic structure of Bi_2Se_3 taken with p-pol. and s-pol. 50 eV photons, respectively. (a3) Corresponding MDCs obtained at $E_b = 0.2$ eV. (b1-b3) Same as in (a1-a3) but for $Bi_{1.78}Cr_{0.22}Se_3$.

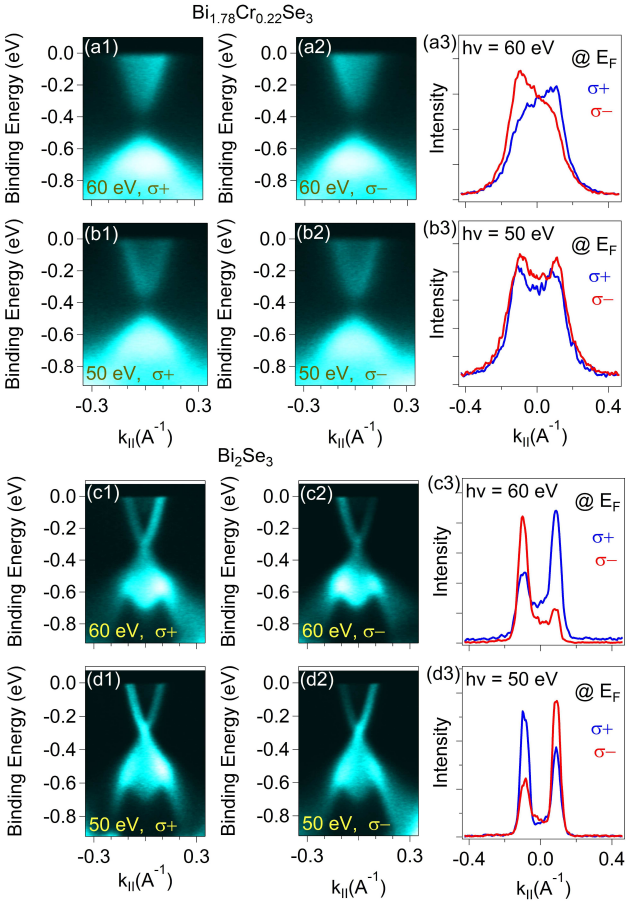

FIG. 5. (a1-a3 and b1-b3) ARPES maps of $Bi_{1.78}Cr_{0.22}Se_3$ obtained with circularly polarized 60 eV and 50 eV photons along with the MDCs integrated within 10 meV at the E_F. (c1-c3 and d1-d3) Same as (a1-a3 and b1-b3) but for Bi_2Se_3.

where E, f, and i are polarization vector of the electric field, final and initial states of the photoexcited electrons, respectively [37-38]. A non-vanishing intensity can be obtained if initial state has the same symmetry as $\mathbf{E} \cdot \mathbf{r}$ [37]. Therefore, ARPES experiments with variable polarized light can probe bands with different symmetries. This approach has been utilized to resolve the orbital composition of the surface states in Bi_2Se_3 and it is found that the TSSs are strongly p_z character with a non-negligibly contribution of p_x and p_y orbitals [33-36]. This can be seen in the upper panel of Figure 4 giving the ARPES map of Bi_2Se_3 obtained with p- and s-polarized lights. In the p-polarized geometry (Figure 4(a1)), the TSSs show a strong spectral weight while it exhibits significantly weaker photoemission intensity in the s-polarized geometry (Figure 4(a2)) indicating the predominant p_z orbital nature of the TSSs in Bi_2Se_3.

To evaluate the impact of the Cr doping on the orbital texture of the surface states, we presented the ARPES maps of $Bi_{1.78}Cr_{0.22}Se_3$ in the lower panel of Figure 4. Similar to pristine Bi_2Se_3, the spectral weight of the surface states in $Bi_{1.78}Cr_{0.22}Se_3$ is dominated by p_z orbitals and also showing non-negligible contribution from the in-plane orbitals. This is deduced from the weakening photoexcited electron intensity by tuning the light polarization from p- (Figure 4(b1)) to s (Figure 4(b2)). Thus, the measurements, here, show that Bi_2Se_3 and $Bi_{1.78}Cr_{0.22}Se_3$ exhibit the similar orbital symmetry. However, there are also differences between the two samples. To visualize this, we presented the momentum dispersion curves (MDCs) at $E_b = 0.2$ eV for Cr doped and pristine samples in Figures 4(a3) and 4(b3), respectively. In Bi_2Se_3, s-polarized light gives only 3 % of photoelectron intensity ejected with the p-polarized light. This ratio, however, is much larger, about 15 % in $Bi_{1.78}Cr_{0.22}Se_3$ (Figure 4(b3)). The difference could be the result of the hybridization between the surface states and the Cr d-orbitals. This prediction is consistent with earlier theoretical reports that the Cr d-orbital lies in the vicinity of the DP [29, 39]. This is in the line with a recent experimental study that the signature for the hybridization between the d bands of the dopant and surrounding states is found in V doped (Bi,Sb)Te by scanning tunneling spectroscopy conducted [53]. Alternatively, Cr doping may modify bulk bands into 2-dimensional electron gas (2DEG) states by the impurity intercalation or the confinement of the bulk bands [49-51]. Whichever the case may be, our observation provides evidence for the modified surface states in Bi_2Se_3 by the impurity bands.

We also conducted circular dichroism-ARPES (CD-ARPES) maps from the Cr doped and the pristine samples by using left ($\sigma-$) and right ($\sigma+$) circularly polarized lights. Figure 5(a1 - a2) gives the experimental surface

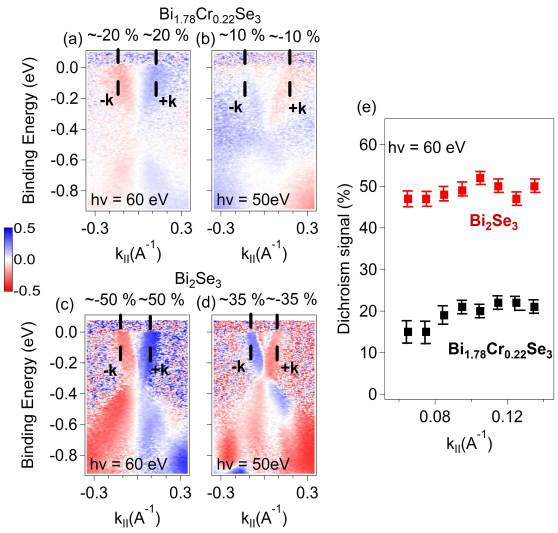

FIG. 6. (a-b) CD-ARPES maps of $Bi_{1.78}Cr_{0.22}Se_3$ taken with circularly polarized 50 eV and 60 eV photons respectively. (c-d) Same as (a1-a2) but for Bi_2Se_3. (e) CD signal of the upper surface states along the $k_\parallel$ for Bi_2Se_3 (red squares) and $Bi_{1.78}Cr_{0.22}Se_3$ (black squares). The CD signal was obtained by integration over the surface states (in momentum) within 20 meV energy window. Each $k_\parallel$ was determined from the corresponding E_b.

electronic structure of the $Bi_{1.78}Cr_{0.22}Se_3$ thin film obtained with circularly polarized 60 eV photons. In Figure 5(a1), above the gap, the electronic structure on the $+\mathbf{k}$ side of the $k_\parallel = 0$ Å^{-1} yields more bright feature than the $-\mathbf{k}$ side for the $\sigma+$ photons. This shows the asymmetric intensity between the left and the right side of the gaped Dirac cone. The photoelectron intensity asymmetry between the left and the right branch of the gapped Dirac cone reverses with tuning polarization from $\sigma+$ to $\sigma-$ while keeping the photon energy at 60 eV as seen in Figure 5(a1) and 5(a2). This can be better distinguished in MDCs presented in Figure 5(a3). in which the right surface state exhibits stronger intensity than the left one for $\sigma+$, and the opposite is observed for the $\sigma-$ 60 eV photons. The switching of the stronger spectral weight between the left and the right surface states is not unique only to the direction of the photon polarization. We also observed the same spectral behavior by tuning photon energy from 60 eV to 50 eV while keeping the photon polarization constant. At 60 eV, the right surface state shows a more intense spectral feature than the left one. This reverses by tuning the photon energy to 50 eV for the same photon polarization as presented in Figure 5(b1)in which the left surface state has stronger spectral intensity than the right one. The same spectral intensity asymmetry switching by tuning the photon energy is also observed $\sigma-$ (Figure 5(a2) and 5(b2)). Another noticeable observation is that the spectral weight difference between the left and the right surface states is much weaker at 50 eV circularly polarized lights compared to the ARPES maps obtained with 60 eV circularly polarized lights. This can be seen in the MDCs given in Figure 5(b3) that the left and right surface states exhibit almost the same height in photoemission intensity peak.

We also applied the same experimental condition to the single crystal Bi_2Se_3. ARPES maps obtained with circularly polarized 60 eV and 50 eV lights along with corresponding MDCs are presented in Figure 5(c1-c3) and 5(d1-d3), respectively. Spectral weight switching between the left and the right side of the $k_\parallel = 0$ Å^{-1} exhibits the same tendency with the Cr doped thin film sample. Such that, the spectral asymmetry of the surface states located on the $-\mathbf{k}$ and $+\mathbf{k}$ momentum regions switches by changing the photon energy as seen between Figure 5(c1) - 5(d1) and Figure 5(c2) - 5(d2) and with photon polarization as given in Figure 5(c1) - 5(c2) and Figure 5(d1) - 5(d2). These observations are supported by the MDCs presented in Figure 5(c3) and 5(d3). However, the spectral weight difference between the left and the right surface states in Bi_2Se_3 is much stronger than the Cr doped thin film sample for the same experimental geometry.

For the quantitative evolution of the CD signal, we presented CD-ARPES maps in Figure 6(a-d) with a color representation in which red and blue indicates the negative and positive values, respectively. The magnitude of the circular dichroism is given by CD = $[(I_{\sigma+} - I_{\sigma-})]/[(I_{\sigma+} + I_{\sigma-})]$ where $I_{\sigma+}$ and $I_{\sigma-}$ are the photoemission intensities obtained with $\sigma+$ and $\sigma-$ lights, respectively. The similarities between the two samples are that the CD signal reverses sign between the left and the right side of the $k_\parallel = 0$ Å^{-1} when photon energy is tuned from 60 eV to 50 eV as well as with changing the photon polarization at fixed photon energy. Furthermore, both samples do not show inversion in the CD sign across the gap in $Bi_{1.78}Cr_{0.22}Se_3$ and the DP in Bi_2Se_3 at 60 eV photon energy. This is seen as the CD exhibits the same asymmetry above and below the gap ($Bi_{1.78}Cr_{0.22}Se_3$) and across the DP (Bi_2Se_3) on the $-\mathbf{k}$ and $+\mathbf{k}$ momentum regions. At 50 eV photon energy, the opposite is true that the CD sign switches across the gap in $Bi_{1.78}Cr_{0.22}Se_3$ and the DP in Bi_2Se_3. Hence, both samples show identical photon energy dependent CD. Another notable feature in CD-ARPES is that both samples possess a nodal line (vanishing CD seen as white color) along the $k_\parallel = 0$ Å^{-1}. This is more evident on the CD-ARPES obtained with 60 eV photons. The nodal line can be taken as a characteristic feature of the TSSs as a consequence of its mirror symmetric effective Hamiltonian [40-44].

As noted before, the Cr doped sample exhibits smaller CD signal than the pristine sample which is quantified in Figure 6(e) demonstrating the CD signal of the surface states as a function of $k_\parallel$. With Cr doping, CD signal drops from ∼50% to ∼20% in Bi_2Se_3. Several factors can lead to the weakening of the CD signal. First, Cr substitution with Bi can reduce SOC strength [21]. But, the materials with very weak SOC also show a strong CD signal as observed in graphene [45]. Nevertheless,

the measured CD signal in the Cr doped Bi_2Se_3 sample is still much stronger than the expectations when it is compared to ferromagnets in which the CD signal is less than 3% [46-47]. Therefore, the variation in SOC strength should not play a dominant role. Furthermore, in a recent work, SOC was found not to cause a strong CD signal in TIs, but its correlation with dipole transition and final state effect in photoemission is proposed to be the major factor in the large magnitude of the CD signal in TIs [48]. Also, the complexity of the CD behavior with nodal line and inversion with photon energy and polarization is proposed to be originated from the strong SOC and the non-trivial orbital texture [48] suggesting that that the Cr doped Bi_2Se_3 possesses topologically non-trivial electronic structure. Another possible origin of the weakened CD could be the modified orbital texture of the surface states. This provides an experimental evidence that the surface states of Cr doped Bi_2Se_3 could be composed of not only the Bi and Se p-orbitals but also a contribution from the Cr d-orbitals. This interpretation is consistent with our photoemission experiment performed with linearly polarized lights (Figure 4b1-b3)) and with earlier theoretical reports [29, 39] stating the existence of the impurity bands near the DP.

Non-dispersive states observed in our work could be associated with the emergent of 2DEG states due to the detachment of the top QL [49]. In this case, an energy gap can be opened at the DP by the hybridization of the surface states across the separated QL [52]. This possibility can retain the non-trivial band topology, while making surface states being 2DEG which still exhibits strong CD. However, this mechanism requires van-der-Walls (vdW) gap to be expanded between 20 and 50 % due to the intercalation of the Cr impurities within the vdW gap. On the other hand, it has been shown by x-ray photoemission spectroscopy and x-ray diffraction experiment that the Cr atoms is substituted with Bi and this does not change the c-lattice parameter of Bi_2Se_3. Therefore, Therefore, Cr doping into the bulk of Bi_2Se_3 could not drive the new surface states.

Furthermore, the sample thickness could be also a reason for the weak CD signal since our Cr doped Bi_2Se_3 is only 3 QL. C. Z. Xu et al. studied such thickness impact on the CD signal of Bi_2Te_3 in Ref. 48. They have found that the CD signal nearly independent of sample thickness at 50 eV photon energy. Therefore, the weakening of the CD signal upon deposition of the Cr impurities is not likely to be originated from the thickness of the sample.

In summary, we presented a detailed ARPES experiment on Cr doped Bi_2Se_3 under the variable experimental geometry. We have found that the Cr doping in Bi_2Se_3 leads to the suppression of the CD signal. Since the two sets of ARPES experiments were performed under the same experimental geometry, the modification of the orbital texture of the surface states could be the main factor behind the weakening of the CD signal. This reveals the spectral contribution Cr d-orbitals to the surface states in Bi_2Se_3. However, further calculations are required to understand such a strong modification of the surface states and the CD-signal in the doped TIs. Moreover, our comparative study on Cr doped Bi_2Se_3 and pristine Bi_2Se_3 provides an experimental signature that the Cr doping does not induce a topological phase transition even for high Cr doping level. The CD-ARPES experiment revealed that the transition metal doping could be an experimental approach for controlling the spin-orbital texture of the TSSs for application in spintronic devices.

This work was funded by the University of Connecticut under the UCONN-REP (Grant No. 4626510) and also by the Institute for Materials Science and LDRD XWNK at Los Alamos National Laboratory. This research also used resources ESM (21ID-I) beamline of the National Synchrotron Light Source II, a U.S. Department of Energy (DOE) Office of Science User Facility operated for the DOE Office of Science by Brookhaven National Laboratory under Contract No. DE-SC0012704. We have no conflict of interest, financial or other to declare. T. Yilmaz thanks A. V. Balatsky for helpful discussions.

[1] L. Fu et al., Phys. Rev. Lett. 98, 106803 (2007).
[2] H. Zhang et al., Nature Phys. 5, 438 (2009).
[3] R. Roy, Phys. Rev. B 79, 195322 (2009).
[4] J. E. Moore, Nature (London) 464, 194 (2010).
[5] J. E. Moore and L. Balents, Phys. Rev. B 75, 121306 (2007).
[6] C. X. Liu et al., Phys. Rev. B 82, 045122 (2010).
[7] L. Fu and C. L. Kane, Phys. Rev. B 76, 045302 (2007).
[8] H. Zhang et al., Phys. Rev. Lett. 111, 066801 (2013).
[9] X. L. Qi and S. C. Zhang, Rev. Mod. Phys. 83, 1057 (2011).
[10] Y. L. Chen et al., Science 325, 178 (2009).
[11] D. Hsieh et al., Nature (London) 460, 1101 (2009). a.
[12] Y. Xia et al., Nature Phys. 5, 398 (2009).
[13] R. Yu et al., Science 329, 61 (2010).
[14] F. D. M. Haldane, Phys. Rev. Lett. 61, 2015 (1988).
[15] C. Z. Chang et al., Nat. Mater. 14, 473 (2015).
[16] C. Z. Chang et al., Science 340, 167 (2013).
[17] W. Li et al., Sci. Rep. 6, 32732 (2016).
[18] L. A. Wray et al., Nature Phys. 7, 32 (2011).
[19] Y. L. Chen et al., Science 329, 659 (2010).
[20] M. Liu et al., Phys. Rev. Lett. 108, 036805 (2012).
[21] J. Zhang et al., Science 339, 1582 (2013).
[22] D. M. Zhang et al., Phys. Rev. B 86, 205127 (2012).
[23] S. Y. Xu et al., Nat. Phys. 8, 616 (2012).
[24] T. Schlenk et al., Phys. Rev. Lett. 110, 126804 (2013).
[25] T. Yilmaz et al., Appl. Surf. Sci. 407, 371 (2017).
[26] T. Yilmaz et al., Phys. Chem. Chem. Phys. 20 8624 (2018).
[27] L. Zhang et al., APL Mater. 5, 076106 (2017).
[28] Y. H. Choi et al., J. Apply. Phys. 109, 07E312 (2011).
[29] J. Bouaziz et al., Phys. Rev. B 98, 035119 (2018).
[30] J. Snchez-Barriga et al., Nat. Commun. 7, 10559 (2016).
[31] A. M. Black-Schaffer and A. V. Balatsky, Phys. Rev. B

86, 115433 (2012).
[32] A. M. Black-Schaffer and A. V. Balatsky, Phys. Rev. B 85, 121103 (2012).
[33] Z. Xie et al., Nat. Commun. 5, 3382 (2014).
[34] Y. Cao et al., Nat. Phys. 9, 499 (2013).
[35] C. Jozwiak et al., Nat. Phys. 9, 293 (2013).
[36] Z. H. Zhu et al., Phys. Rev. Lett. 110, 216401 (2013).
[37] S. Hfner, Photoelectron Spectroscopy: Principles and Applications (Springer, Berlin, 2003).
[38] W. Eberhardt and F. J. Himpsel, Phys. Rev. B 21, 5572 (1980).
[39] M. F. Islam et al., Phys. Rev. B 97, 155429 (2018).
[40] F. Vidal et al., Phys. Rev. B 88, 241410 (2013).
[41] Y. Ishida et al., Phys. Rev. Lett. 107, 077601 (2011).
[42] M. R. Scholz et al., Phys. Rev. Lett. 110, 216801 (2013).
[43] S. Soltani et al., Phys. Rev. B 95, 125103 (2017).
[44] V. B. Zabolotnyy et al., Phys. Rev. B 76, 024502 (2007).
[45] Y. Liu et al., Phys. Rev. Lett. 107, 166803 (2011).
[46] W. Kuch and C. M. Schneider, Rep. Prog. Phys. 64, 147 (2001).
[47] G. Schnhense, Phys. Scr. T 31, 255 (1990).
[48] C. Z. Xu et al., Phys. Rev. Lett. 115, 016801 (2015).
[49] S. V. Eremeev et al., New J. Phys. 14, 113030 (2012).
[50] M. Bianchi et al., Nature Commun. 1, 128 (2010).
[51] M. S. Bahramyet al., Nat. Commun. 3, 1159 (2012).
[52] Y. Zhang et al., Nature Phys. 6, 584 (2010).
[53] T. Xu et al., Phys. Rev. B 99, 094308 (2019).